RZ 3936 (# ZUR1709-019) 09/11/2017
Physical Sciences 7 pages

Research Report

Room-Temperature Lasing from Monolithically Integrated GaAs Microdisks on Silicon

Stephan. Wirths[1], Benedikt F. Mayer, H. Schmid, Marilyne Sousa, Johannes Gooth[2], Heike Riel, Kirsten E. Moselund

IBM Research – Zurich
8803 Rüschlikon
Switzerland

[1]Present address:
ABB Switzerland Ltd. Corporate Research,
CH-5405 Baden-Daettwil
Switzerland.

[2] Present address:
Max Planck Institute for the Chemical Physics of Solids
01187 Dresden
Germany.

This article has been published in *ACS Nano* **2018** *12* (3), 2169-2175
DOI: 10.1021/acsnano.7b07911 as an open access article under an ACS AuthorChoice License, which permits copying and redistribution of the article or any adaptations for non-commercial purposes.

ACS NANO

Cite This: ACS Nano 2018, 12, 2169–2175

www.acsnano.org

ARTICLE

Room-Temperature Lasing from Monolithically Integrated GaAs Microdisks on Silicon

Stephan Wirths,*,†,‡ Benedikt F. Mayer,‡ Heinz Schmid, Marilyne Sousa, Johannes Gooth,§ Heike Riel, and Kirsten E. Moselund*

IBM Research–Zürich, Säumerstrasse 4, 8803 Rüschlikon, Switzerland

Supporting Information

ABSTRACT: **Additional functionalities on semiconductor microchips are progressively important in order to keep up with the ever-increasing demand for more powerful computational systems. Monolithic III–V integration on Si promises to merge mature Si CMOS processing technology with III–V semiconductors possessing superior material properties, *e.g.*, in terms of carrier mobility or band structure (direct band gap). In particular, Si photonics would strongly benefit from an integration scheme for active III–V optoelectronic devices in order to enable low-cost and power-efficient electronic–photonic integrated circuits. We report on room-temperature lasing from AlGaAs/GaAs microdisk cavities monolithically integrated on Si(001) using a selective epitaxial growth technique called template-assisted selective epitaxy. The grown gain material possesses high optical quality without indication of threading dislocations, antiphase boundaries, or twin defects. The devices exhibit single-mode lasing at $T < 250$ K and lasing thresholds between 2 and 18 pJ/pulse depending on the cavity size (1–3 μm in diameter).**

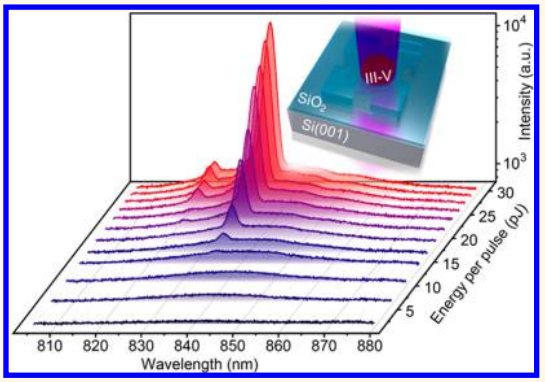

KEYWORDS: *direct epitaxy, monolithic III–V laser integration, template-assisted selective epitaxy, III–V on Si, microdisk lasers, room-temperature lasing*

We recently entered the zettabyte era; that is, the annual global Internet data traffic passed 1000 exabytes (1 billion terabytes). Until the year 2020 this number will even increase to 2.3 zettabytes every year,[1] however, at the expense of a drastically increased power consumption of integrated circuits (ICs). Moreover, since 2016, the semiconductor industry research plan is not centered on device scaling anymore, *i.e.*, improving the chip performance followed by the application. Thus, the integration of additional, value-added functionalities on future silicon dies and reducing the power consumption at the same time will be key for upcoming strategies, which will start with the application defining the functionality of future Si-based chips.[2] This in turn will require the integration of a large variety of devices such as amplifiers, ultralow power switches, and especially optoelectronic devices on the very same Si substrate to benefit from the maturity and low cost of the CMOS technology platform. In particular, approaches including the usage of massless photons instead of electrons for the data transfer on- and off-chip promise higher speed at lower power consumption.[3,4] In order to shed light on Si chips and make such electronic–photonic integrated circuits (EPICs) a reality, high-performance waveguides,[5] modulators,[6] and photodetectors[7] in Si or group IV photonics have already been developed. However, the deleterious impact of threading dislocations introduced by the lattice mismatch between Si and III–V material has strongly complicated the realization of coherent on-chip laser sources being the last missing piece to enable fully integrated EPICs. In this context, the most obvious solution would be to use group IV materials, where Ge as well as its alloys with Sn plays a primary role, due to the possibility to turn them into direct band gap semiconductors and gain media.[8−10] Very recently, direct band gap $Ge_{1-x}Sn_x$ epilayers with $x < 0.13$ and optically pumped GeSn laser devices were demonstrated.[11,12] However, electrically pumped lasing at room temperature in direct band gap group IV semiconductors is still rather challenging. III–V electrically pumped lasers are well-established for telecommunication and other applications, but the large-scale integration of III–V laser diodes on a Si platform is hampered by various obstacles, although significant progress was achieved in heterogeneous and monolithic integration of III–V gain material on Si.[13−17] Since traditional heteroepitaxy typically suffers from large differences of the crystal lattices and thermal expansion—resulting in defective layers—several techniques were developed in order to suppress and/or confine the

Received: November 7, 2017
Accepted: January 24, 2018
Published: January 24, 2018

DOI: 10.1021/acsnano.7b07911
ACS Nano 2018, 12, 2169–2175

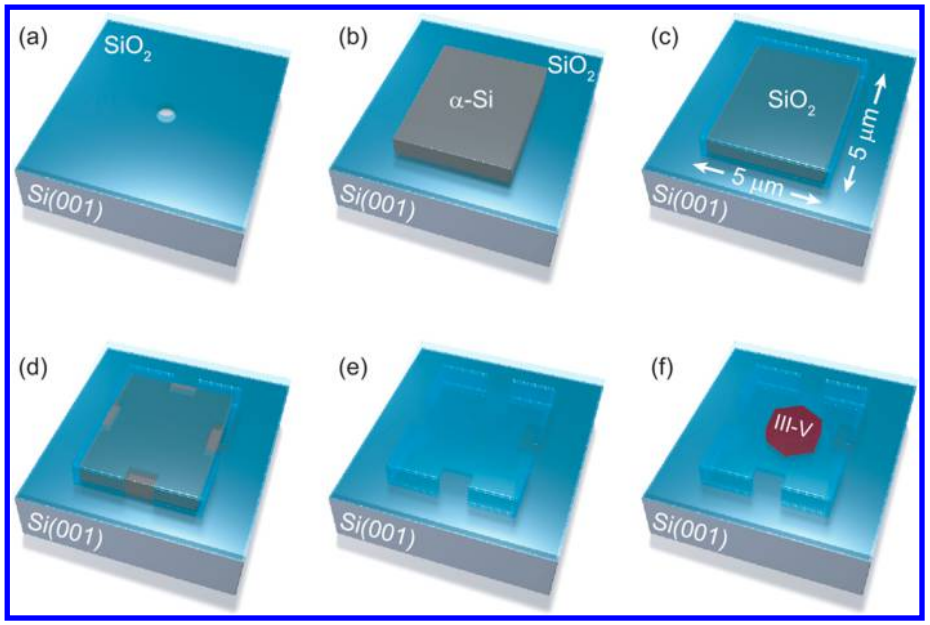

Figure 1. Fabrication of the GaAs microdisk laser. (a) Etching holes in a thermally oxidized Si(001) wafer using an RIE dry etching step. (b) Deposition and patterning of amorphous Si (α-Si). (c) Covering of the α-Si with ALD (20 nm) and PECVD (120 nm) SiO_2. (d) Patterning and RIE etching of template openings. (e) Selective etching of the sacrificial α-Si layer using XeF_2. (f) Finally, the hollow SiO_2 cavities are filled using selective epitaxy (MOCVD).

defective interface layer close to the substrate and ensure a nearly defect-free device layer. This includes the growth of thick buffer layers,[18−21] nanowires,[13,15] and/or masked substrates[22] that leads to a significantly reduced density of crystal defects and dislocations. A promising integration path was recently demonstrated using selective area growth in trenches[22] and in prepatterned V-grooves,[23] which resulted in an optically and electrically driven laser on Si(001), respectively. Another approach is based on bonding of *ex-situ* fabricated III−V photonic components,[16] which recently made significant progress regarding yield and device lifetime.[24]

In this paper, we present the monolithic integration of III−V semiconductors for photonic devices on Si, based on a selective epitaxial growth technique (template-assisted selective epitaxy, TASE) that had been successfully developed for nanoelectronic devices.[25−28] The basic concept relies on the idea of a single and small-area nucleation of the III−V material on Si—with any substrate orientation—within hollow SiO_2 template structures of arbitrary shapes. This procedure allows for direct III−V heteroepitaxy on Si without typical defects such as threading dislocations or antiphase boundaries, avoiding the usage of thick buffer layers, and, thus, could enable large-scale optoelectronics integration. A necessity of adapting the TASE process to photonic devices, though, is to increase the dimensions of the templates and resulting III−V structures while maintaining the material quality. Here we report on optimized template designs, fabrication steps, and active materials compared to the nanoelectronics analogue[25,29] and demonstrate the integration of AlGaAs/GaAs microdisk structures as active photonic devices. Optically pumped lasing up to room temperature is achieved along with temperature-stable lasing threshold and lasing peak position.

RESULTS AND DISCUSSION

Laser Fabrication. In order to monolithically integrate III−V semiconductor gain material, we employ the TASE growth technique presented and discussed elsewhere.[25,26,30] This approach promises nearly defect-free heteroepitaxy of III−V material on Si substrates. As laser gain material GaAs with an AlGaAs cladding deposited by MOCVD is used. The fabrication steps of the GaAs/AlGaAs microdisk devices are illustrated in Figure 1. Standard Si(001) substrates are used and thermally oxidized (approximately 130 nm SiO_2 oxide thickness) to provide a high refractive index mismatch between the GaAs (n_{GaAs} = 3.6) and the surrounding medium (n_{SiO2} = 1.5), thus enabling a simulated cavity Q-factor of ∼730. Subsequently, holes (100 nm diameter) were etched through the oxide using a CHF_3/O_2 reactive ion etching (RIE) dry etch process as shown schematically in Figure 1a. Next, an etch stop layer of 2−3 nm Al_2O_3 as well as a sacrificial amorphous Si (α-Si) layer were deposited. A 5 × 5 μm^2 mesa structure centered on top of the etched holes was patterned using e-beam lithography and an HBr/O_2-based inductively coupled plasma (ICP) etch process (see Figure 1b). These squares were covered with SiO_2 (which is called a template in the following) using atomic layer deposition (ALD, 20 nm) and plasma-enhanced chemical vapor deposition (PECVD, 120 nm), and four template openings are defined and etched into the oxide as indicated in Figure 1c and d. The size and shape of the openings ensure efficient precursor supply during growth while mechanically stabilizing the hollow oxide template. Afterward the sacrificial Si inside the templates and holes is etched (see Figure 1e) using XeF_2. Prior to the metalorganic chemical vapor deposition (MOCVD) growth step (Figure 1f) the Al_2O_3 etch stop layer as well as the native SiO_2 were etched using BHF while forming a hydrogen passivation on the Si surface. We grew two different samples for this study; both growth processes start with GaAs growth at 600 °C and a V−III ratio of 30 (sample A, 90 min; sample B, 30 min) using trimethylgallium (TMGa) and *tert*-butylarsine (TBAs) finalized with an AlGaAs/GaAs shell adding trimethylaluminum (TMAl). Whereas microdisk devices from sample B are approximately 1 μm in diameter, cavities from sample A are typically 3 times larger.

DOI: 10.1021/acsnano.7b07911
ACS Nano 2018, 12, 2169−2175

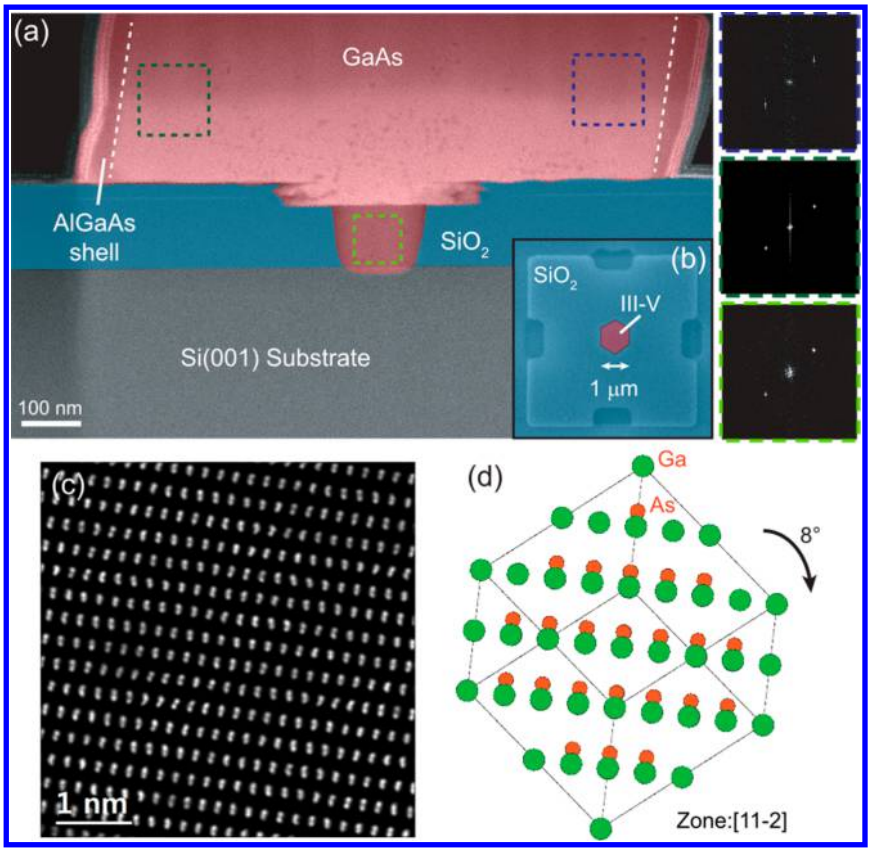

Figure 2. (a) Cross-sectional ADF-STEM image of a microdisk from sample B. The insets display the fast Fourier transform images from the left and right segments as well as from the seed of the GaAs crystal. (b) Top-view scanning electron micrograph of the investigated device. (c) ADF-STEM micrograph along the [11−2] direction after high-frequency noise reduction using a Gaussian low-pass filter for noise reduction. (d) Ball-and-stick model of the GaAs crystal along the [11−2] direction.

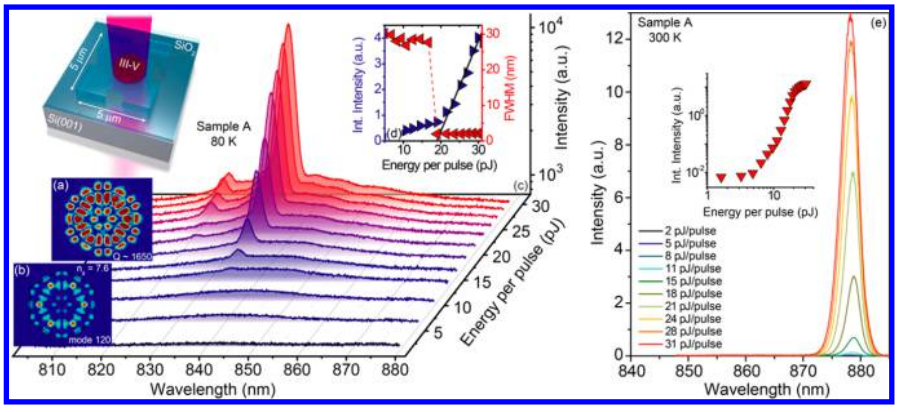

Figure 3. (a, b) 3D FDTD and 2D mode simulations, respectively, indicating higher order modes (mode 120), a group index of 7.6, and a Q-factor of 1650. (c) Photoluminescence (PL) spectra of a 3 μm device measured at 80 K. The inset shows a schematic view of the optical excitation and light detection. (d) Light-in light-out curve as well as the fwhm as a function of excitation at 80 K. (e) Room-temperature PL spectra and light-in light-out curve (inset) of another device from sample A.

Morphological Analysis. In order to investigate the crystalline quality, orientation, and the seed area, we cut out several TEM lamellas from microdisk devices using Ga focused-ion beam (FIB) etching at accelerating voltages of 30 and 5 kV. The samples were investigated by scanning transmission electron microscopy (STEM) using a double spherical aberration corrected JEOL ARM200F operating at 200 kV and equipped with a JEOL Dry SD100GV silicon drift detector with 100 mm^2 detection area for energy dispersive X-ray spectroscopy (EDX) analyses. The chemical maps obtained by EDX are presented in the Supporting Information, Figure S1, while annular dark field (ADF) images are shown in Figure 2. For those images, a convergence semiangle of 25 mrad was used in combination with an ADF detector with inner and outer collection semiangles of 90 and 370 mrad, respectively. Images obtained with an ADF are shown in Figure 2, while EDX images are presented in the Supporting Information, Figure S1.

In Figure 2a a cross-sectional STEM of a microdisk from sample B is presented and a top-view scanning electron

DOI: 10.1021/acsnano.7b07911
ACS Nano 2018, 12, 2169−2175

micrograph (SEM) of the same device is shown in Figure 2b. This is the device on which we carried out the optical characterization presented in Figures 4 and 5. The disk radius is approximately 1 μm, whereas its thickness and the oxide thickness underneath amount to ~335 nm and ~140 nm, respectively. Following the various processing and wet etching steps, the seed hole diameters are typically slightly extended and measure approximately 120 nm. The contrast gradient across (top to bottom) the GaAs region originates from a thickness variation from the sample preparation. Moreover, several Ga residues are visible as dark spots. The high-resolution ADF-STEM micrographs as well as their fast Fourier transform images (insets of Figure 2a) reveal identical crystal orientation throughout the entire III–V crystal, denoting monocrystalline growth without amorphous or polycrystalline segments. Moreover, we do not observe any crystal defects such as threading dislocations, antiphase boundaries, or planar defects for this laser device. For this study we investigated seven devices, and Figure S2 shows an example of a nonlasing device. For in-depth planar defect analysis of TASE-grown GaAs, we refer to our recent work.[31] The top-view SEM image (Figure 2b) shows well-defined facets. However, the entire crystal is tilted by 8° and rotated toward the (11−2) plane, as shown in Figure 2d, compared to the Si substrate. We believe that this unexpected tilt and rotation of the crystal might stem from a damaged Si surface from RIE overetching, as evidenced by the noticeable Si recess in the seed hole as well as the observation of defective crystals as shown in Figure S2.

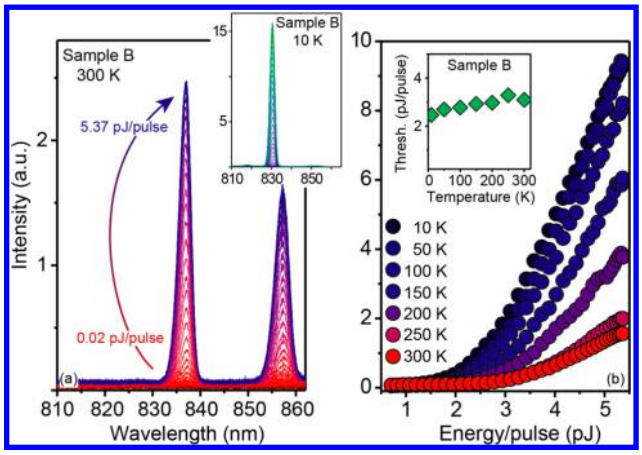

Figure 4. Optical characteristics of MD lasers from sample B at (a) room temperature and 10 K (see inset). (b) Temperature-dependent light-in light-out curves. The temperature-dependent lasing threshold is shown in the inset.

Optical Characterization of the GaAs/AlGaAs/GaAs Microdisk Lasers. The microdisk resonators were optically excited using a pulsed (15 ps pulse length every 10 ns) supercontinuum laser with center wavelengths of 705 and 710 nm close to the expected laser emission of the devices. The emission is collected from the top. A scheme of the measurement procedure is illustrated in the inset of Figure 3c. According to 3D finite difference time domain (FDTD) simulations of the cavity field decay using randomly oriented dipole emitters (see Supplementary Figure S4) and disk dimensions extracted from the TEM results, a clear mode profile is established, as presented in Figure 3a. The enhanced reflectivity of the high-order mode supported by the 3 μm nanodisk cavity[32] and the high refractive index mismatch between the GaAs nanodisk and the surrounding media results in a simulated cavity Q-factor of 1650. Additionally, 2D mode simulations using a commercial Helmholtz equation solver (Lumerical) show that a high-order (120) mode displayed in Figure 3b resembles the mode profile found with the FDTD simulation using the random-dipole method. Figure 3c shows photoluminescence (PL) spectra with a spectral resolution of ~0.1 nm as a function of optical excitation at 80 K for a 3 μm microdisk device. Whereas the spontaneous emission dominating at low excitations is centered around 840 nm—being in good agreement with the low-temperature GaAs band gap—whispering gallery modes (WGM) appear above an excitation of 15 pJ per pulse. The integrated PL intensity as a function of excitation—light-in light-out (LL) curve—exhibits a clear kink along with a strong line width reduction at a lasing threshold of 18 pJ/pulse (see Figure 3d). Another device from sample A, shown in Figure 3e, exhibits lasing even up to room temperature with a similar lasing threshold. The corresponding LL curve features a typical S-shape behavior, which, accompanied by the strong line width narrowing, constitutes

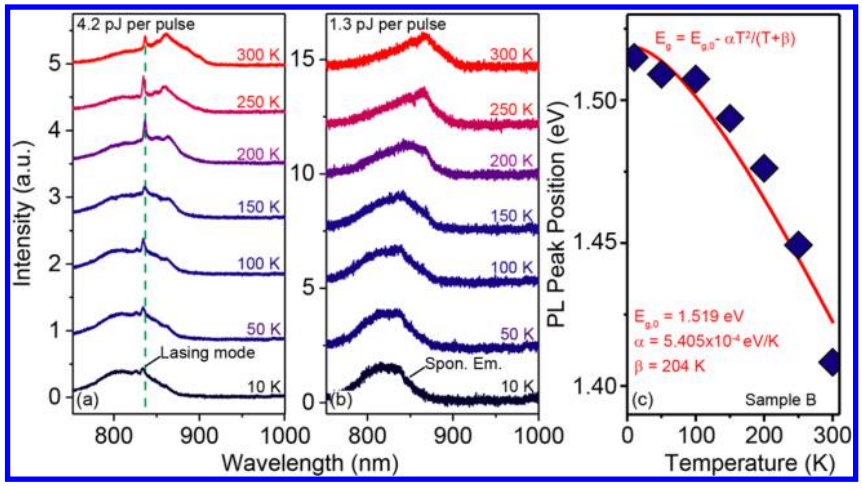

Figure 5. Temperature-dependent PL spectra (a) above the lasing threshold at 4.2 pJ per pulse and (b) below the lasing threshold at 1.3 pJ per pulse of a device from sample B. (c) PL peak position as a function of temperature following Varshni's law.

DOI: 10.1021/acsnano.7b07911
ACS Nano 2018, 12, 2169–2175

a clear signature of the room-temperature lasing operation of the device.

The temperature-dependent optical characterization of a microdisk laser device from sample B is presented in Figure 4. This monocrystalline device (*cf.* Figure 2) is 1 μm in diameter with a thickness of approximately 335 nm. The excitation-dependent room-temperature as well as low-temperature (10 K) PL spectra are displayed in Figure 4a and its inset, respectively. We found that the lasing thresholds of these smaller devices extracted from the LL curves (Figure 4b) are significantly lower (2.5−3.0 pJ/pulse) compared to the values observed for devices from sample A. Comparing the lasing thresholds measured for the 1 μm (2 pJ/pulse) and the 3 μm (18 pJ/pulse) microdisks we find a ∼9× higher lasing threshold for the large devices. As both devices are fabricated under the same growth conditions, we expect similar material qualities. Therefore, we conclude that either the different cavity confinement or simply the 9× larger gain volume of the 3 μm disk is responsible for the enhanced pumping energy required for the lasing operation of the larger device. The FDTD simulations presented in Figure S4 show that the cavity Q factor of the 1 μm disk (Q = 1430) and Q factor of the 3 μm disk (Q = 1650) are very similar. Since we optimized the laser spot size for the maximum photoluminescence intensity for each of the devices, we assume a constant excitation power per area for a given excitation laser power. Therefore, we believe that the 9× higher lasing threshold measured for the large device is mainly related to the scaling (9×) of the gain material volume, which is in excellent agreement with our experimental results. Remarkably, we observed that between 10 and 300 K the lasing peak position moves only very slightly from 830 to 836 nm (see Figure 5a), whereas the peak of the spontaneous emission follows Varshni's law. Furthermore, we observe single-mode operation without any mode hopping up to 250 K and attribute the maximum shift of the lasing mode, $\Delta\lambda_T$ = 6 nm, to the temperature-induced refractive index change.[33] However, at room temperature, multimode lasing operation with a free spectral range (FSR) of 20 nm as shown in Figure 4a is observed. Additionally, as shown in the inset of Figure 4b, the lasing threshold is very insensitive to changes of the lattice temperature and increases only marginally from 2.5 pJ/pulse to 3.0 pJ/pulse for a temperature increase from 10 K to 300 K, corresponding to an extremely high characteristic temperature of T_0 = 1500 K, which is more than 1 order of magnitude larger than for III−V quantum dot microdisk lasers.[33−35] We believe that due to the small diameter of the device and, thus, large FSR, only one (T < 250 K) or two modes (300 K) lie within the gain spectrum while providing sufficiently low cavity losses to enable lasing. As can be seen in Figure 5a, the spontaneous emission curve exhibits a very broad fwhm of ∼70 nm even at 10 K and shows a very strong high-energy tail that extends far beyond 800 nm. This slow decay of the high-energy tail cannot only be explained by thermal carrier activation, which corresponds to k_BT = 0.86 meV (0.5 nm) at 10 K and, therefore, is a clear signature for an inequilibrium between the lattice temperature and the carrier temperature in the gain material caused by, for example, electron−electron collisions. However, as can be seen in Figure 5a, this strong spectral broadening of the material gain is very beneficial for the temperature stability of the device, as despite the Varshni shift and thermal depopulation, the overlap of the material gain and lasing cavity mode remains high if the temperature is increased.

CONCLUSION

In summary, we demonstrated the monolithic integration of GaAs-based microdisk lasers on Si using template-assisted selective epitaxy. We developed a template process and design that enables the direct epitaxy of monocrystalline, μm-large III−V microdisks on Si(001) with high optical quality. The devices show unambiguous lasing action up to room temperature with thresholds between 2 and 18 pJ/pulse depending on the cavity size. Thus, TASE-grown gain materials and photonic devices on Si(001) represent a promising large-scale integration path toward electrically actuated lasers for merging electronics with photonics in order to reduce power consumption, *i.e.*, *via* optical interconnects, and to enrich the functionality of future Si ICs.

METHODS

The AlGaAs/GaAs growth was conducted in a Veeco P150 MOCVD system at 60 Torr using H_2 carrier gas, TMGa, TMAl, and TBAs as precursors. Prior to loading, the samples were etched in diluted hydrofluoric acid (HF) in order to remove the native oxide on the Si seed surface within the templates. Typical growth times were between 60 and 90 min. The dimensions of the AlGaAs/GaAs microdisks were measured after growth by inspection in a Hitachi SU8000 SEM. For the optical characterization of the microdisk lasers we used a home-built microphotoluminescence setup. The samples were excited using a pulsed supercontinuum light source with a repetition rate of 80 MHz and a typical pulse duration of 10 ps, which was filtered to a 5 nm spectral window around 720 nm. In order to reduce the degradation of the structures subject to the excitation light, we employed a chopper wheel to reduce the total number of excitation pulses by a factor of approximately 40. To avoid parasitic signals from the excitation source in the wavelength range of the microdisk emission between 800 and 900 nm, we used a 750 nm short-pass filter in the excitation path and a 750 nm long-pass filter in the detection path. The excitation light was focused onto the sample using a 50× Olympus objective, and the photoluminescence signal was collected with the same objective mounted inside a He-flow cryostat underneath a window opening, which provides optical access. The samples were glued onto the coldfinger, which can be moved in the x- and y-direction using a closed-loop piezo actuator stage. The objective can be moved in the z-direction using another piezo actuator to adjust the focus. The photoluminescence spectra of the microdisks were recorded using a liquid nitrogen cooled InGaAs line detector array with 1024 pixels mounted to a spectrometer with a focal length of 500 mm and an 850/mm grating. The photoluminescence signal is guided to the spectrometer and focused to the entrance slit with a width of ∼25 μm. An imaging system consisting of a halogen light source to illuminate the sample, a 20 cm lens to focus the image of the sample onto a CCD camera, a beam splitter to separate the two optical paths, and a semitransparent pellicle to add the imaging system to the excitation and detection paths was used to provide orientation on the sample and to record images of the microdisk emission using a 750 nm long-pass filter in front of the CCD. Samples for transmission electron microscopy were prepared by means of a dual-beam focused FEI Helios Nanolab 450S FIB. The samples were subsequently investigated by STEM using a double spherical aberration corrected JEOL ARM200F operating at 200 kV equipped with a JEOL Dry SD100GV silicon drift detector with 100 mm^2 detection area for EDX analyses. ADF images were taken using a convergence semiangle of 25 mrad in combination with an ADF detector with inner and outer collection semiangles of 90 and 370 mrad, respectively.

ASSOCIATED CONTENT

Supporting Information

The Supporting Information is available free of charge on the ACS Publications website at DOI: 10.1021/acsnano.7b07911.

DOI: 10.1021/acsnano.7b07911
ACS Nano 2018, 12, 2169−2175

Additional information on TEM and EDX analyses as well as FDTD simulations (PDF)

AUTHOR INFORMATION

Corresponding Authors

*E-mail: stephan.wirths@ch.abb.com.
*E-mail: kmo@zurich.ibm.com.

ORCID

Stephan Wirths: 0000-0002-3462-7640
Heinz Schmid: 0000-0002-0228-4268
Johannes Gooth: 0000-0002-4062-3232

Present Addresses

†ABB Switzerland Ltd. Corporate Research, CH-5405 Baden-Daettwil, Switzerland.
§Max Planck Institute for the Chemical Physics of Solids, Noethnitzer Straße 40, 01187 Dresden, Germany.

Author Contributions

‡S. Wirths and B. F. Mayer contributed equally to this work.

Notes

The authors declare no competing financial interest.

ACKNOWLEDGMENTS

The research leading to these results has received funding from the European Union's Horizon 2020 Research and Innovation Program under Grant Agreement No. 704045 "MODES" (Marie Curie Post-Doctoral Research Fellowship), No. 641023 "NanoTandem", and the ERC Starting Grant project under Grant Agreement No. 678567 "PLASMIC". The authors would also like to thank Dr. M. D. Rossell from the Electron Microscopy Center (EMPA), Dübendorf, Switzerland, for fruitful discussions, S. Reidt for TEM lamella preparation, and M. Tschudy for his support.

REFERENCES

(1) Cisco. The Zettabyte Era: Trends and Analysis http://www.cisco.com/c/en/us/solutions/collateral/service-provider/visual-networking-index-vni/vni-hyperconnectivity-wp.html (accessed Jun 7, 2017).
(2) Waldrop, M. M. The Chips Are down for Moore's Law. *Nature* **2016**, *530*, 144−147.
(3) Green, W.; Assefa, S.; Rylyakov, A.; Schow, C.; Horst, F.; Vlasov, Y. CMOS Integrated Silicon Nanophotonics: An Enabling Technology for Exascale Computing. In *Advanced Photonics*; OSA: Washington, D.C., 2011; p IME1.
(4) Masini, G.; Capellini, G.; Witzens, J.; Gunn, C. A 1550nm, 10Gbps Monolithic Optical Receiver in 130nm CMOS with Integrated Ge Waveguide Photodetector. In *2007 4th IEEE International Conference on Group IV Photonics*; IEEE, 2007; pp 1−3.
(5) Xia, F.; Sekaric, L.; Vlasov, Y. Ultracompact Optical Buffers on a Silicon Chip. *Nat. Photonics* **2007**, *1*, 65−71.
(6) Xu, Q.; Schmidt, B.; Pradhan, S.; Lipson, M. Micrometre-Scale Silicon Electro-Optic Modulator. *Nature* **2005**, *435*, 325−327.
(7) Assefa, S.; Xia, F.; Vlasov, Y. A. Reinventing Germanium Avalanche Photodetector for Nanophotonic on-Chip Optical Interconnects. *Nature* **2010**, *464*, 8813.
(8) Von den Driesch, N.; Stange, D.; Wirths, S.; Mussler, G.; Holländer, B.; Ikonic, Z.; Hartmann, J. M.; Stoica, T.; Mantl, S.; Grützmacher, D.; Buca, D. Direct Bandgap Group IV Epitaxy on Si for Laser Applications. *Chem. Mater.* **2015**, *27*, 4693−4702.
(9) Stange, D.; Wirths, S.; von den Driesch, N.; Mussler, G.; Stoica, T.; Ikonic, Z.; Hartmann, J. M.; Mantl, S.; Grützmacher, D.; Buca, D. Optical Transitions in Direct-Bandgap $Ge_{1-x}Sn_x$ Alloys. *ACS Photonics* **2015**, *2*, 1539−1545.
(10) Stange, D.; Wirths, S.; Geiger, R.; Schulte-Braucks, C.; Marzban, B.; von den Driesch, N.; Mussler, G.; Zabel, T.; Stoica, T.; Hartmann, J.-M.; Mantl, S.; Grützmacher, D.; Buca, D. Optically Pumped GeSn Microdisk Lasers on Si. *ACS Photonics* **2016**, *3*, 1279−1285.
(11) Wirths, S.; Geiger, R.; von den Driesch, N.; Mussler, G.; Stoica, T.; Mantl, S.; Ikonic, Z.; Luysberg, M.; Chiussi, S.; Hartmann, J. M.; Sigg, H.; Faist, J.; Buca, D.; Grützmacher, D. Lasing in Direct-Bandgap GeSn Alloy Grown on Si. *Nat. Photonics* **2015**, *9*, 88−92.
(12) Al-Kabi, S.; Ghetmiri, S. A.; Margetis, J.; Pham, T.; Zhou, Y.; Dou, W.; Collier, B.; Quinde, R.; Du, W.; Mosleh, A.; Liu, J.; Sun, G.; Soref, R. A.; Tolle, J.; Li, B.; Mortazavi, M.; Naseem, H. A.; Yu, S.-Q. An Optically Pumped 2.5 μm GeSn Laser on Si Operating at 110 K. *Appl. Phys. Lett.* **2016**, *109*, 171105.
(13) Mayer, B.; Janker, L.; Loitsch, B.; Treu, J.; Kostenbader, T.; Lichtmannecker, S.; Reichert, T.; Morkötter, S.; Kaniber, M.; Abstreiter, G.; Gies, C.; Koblmüller, G.; Finley, J. J. Monolithically Integrated High-β Nanowire Lasers on Silicon. *Nano Lett.* **2016**, *16*, 152−156.
(14) Mayer, B.; Rudolph, D.; Schnell, J.; Morkötter, S.; Winnerl, J.; Treu, J.; Müller, K.; Bracher, G.; Abstreiter, G.; Koblmüller, G.; Finley, J. J. Lasing from Individual GaAs-AlGaAs Core-Shell Nanowires up to Room Temperature. *Nat. Commun.* **2013**, *4*, 2931.
(15) Saxena, D.; Mokkapati, S.; Parkinson, P.; Jiang, N.; Gao, Q.; Tan, H. H.; Jagadish, C. Optically Pumped Room-Temperature GaAs Nanowire Lasers. *Nat. Photonics* **2013**, *7*, 963−968.
(16) Hofrichter, J.; Morf, T.; Porta, A. La; Raz, O.; Dorren, H. J. S.; Offrein, B. J. A Single InP-on-SOI Microdisk for High-Speed Half-Duplex On-Chip Optical Links. *Opt. Express* **2012**, *20*, B365−B370.
(17) Liang, D.; Fiorentino, M.; Okumura, T.; Chang, H. H.; Spencer, D. T.; Kuo, Y. H.; Fang, A. W.; Dai, D.; Beausoleil, R. G.; Bowers, J. E. Electrically-Pumped Compact Hybrid Silicon Microring Lasers for Optical Interconnects. *Opt. Express* **2009**, *17*, 20355−20364.
(18) Luxmoore, I. J.; Toro, R.; Del Pozo-Zamudio, O.; Wasley, N. A.; Chekhovich, E. A.; Sanchez, A. M.; Beanland, R.; Fox, A. M.; Skolnick, M. S.; Liu, H. Y.; Tartakovskii, A. I. III-V Quantum Light Source and Cavity-QED on Silicon. *Sci. Rep.* **2013**, *3*, 1239.
(19) Groenert, M. E.; Pitera, A. J.; Ram, R. J.; Fitzgerald, E. A. Improved Room-Temperature Continuous Wave GaAs/AlGaAs and InGaAs/GaAs/AlGaAs Lasers Fabricated on Si Substrates *via* Relaxed Graded Ge_xSi_{1-x} Buffer Layers. *J. Vac. Sci. Technol., B: Microelectron. Process. Phenom.* **2003**, *21*, 1064.
(20) Shi, B.; Zhu, S.; Li, Q.; Wan, Y.; Hu, E. L.; Lau, K. M. Continuous-Wave Optically Pumped 1.55 μm InAs/InAlGaAs Quantum Dot Microdisk Lasers Epitaxially Grown on Silicon. *ACS Photonics* **2017**, *4*, 204−210.
(21) Chen, S.; Li, W.; Wu, J.; Jiang, Q.; Tang, M.; Shutts, S.; Elliott, S. N.; Sobiesierski, A.; Seeds, A. J.; Ross, I.; Smowton, P. M.; Liu, H. Electrically Pumped Continuous-Wave III−V Quantum Dot Lasers on Silicon. *Nat. Photonics* **2016**, *10*, 307−311.
(22) Wang, Z.; Tian, B.; Pantouvaki, M.; Guo, W.; Absil, P.; Van Campenhout, J.; Merckling, C.; Van Thourhout, D. Room-Temperature InP Distributed Feedback Laser Array Directly Grown on Silicon. *Nat. Photonics* **2015**, *9*, 837−842.
(23) Norman, J.; Kennedy, M. J.; Selvidge, J.; Li, Q.; Wan, Y.; Liu, A. Y.; Callahan, P. G.; Echlin, M. P.; Pollock, T. M.; Lau, K. M.; Gossard, A. C.; Bowers, J. E. Electrically Pumped Continuous Wave Quantum Dot Lasers Epitaxially Grown on Patterned, on-Axis (001) Si. *Opt. Express* **2017**, *25*, 3927.
(24) Doussiere, P. Laser Integration on Silicon. In *2017 IEEE 14th International Conference on Group IV Photonics (GFP)*; IEEE, 2017; pp 169−170.
(25) Schmid, H.; Borg, M.; Moselund, K.; Gignac, L.; Breslin, C. M.; Bruley, J.; Cutaia, D.; Riel, H. Template-Assisted Selective Epitaxy of III−V Nanoscale Devices for Co-Planar Heterogeneous Integration with Si. *Appl. Phys. Lett.* **2015**, *106*, 233101.
(26) Borg, M.; Schmid, H.; Moselund, K. E.; Signorello, G.; Gignac, L.; Bruley, J.; Breslin, C.; Das Kanungo, P.; Werner, P.; Riel, H. Vertical III-V Nanowire Device Integration on Si(100). *Nano Lett.* **2014**, *14*, 1914−1920.
(27) Czornomaz, L.; Uccelli, E.; Sousa, M.; Deshpande, V.; Djara, V.; Caimi, D.; Rossell, M. D.; Erni, R.; Fompeyrine, J. Confined Epitaxial

DOI: 10.1021/acsnano.7b07911
ACS Nano 2018, 12, 2169−2175

Lateral Overgrowth (CELO): A Novel Concept for Scalable Integration of CMOS-Compatible InGaAs-on-Insulator MOSFETs on Large-Area Si Substrates. *VLSI Technol. (VLSI Technol. 2015 Symp.* **2015**, *xx*, T172−T173.
(28) Borg, M.; Schmid, H.; Moselund, K. E.; Cutaia, D.; Riel, H. Mechanisms of Template-Assisted Selective Epitaxy of InAs Nanowires on Si. *J. Appl. Phys.* **2015**, *117*, 144303.
(29) Cutaia, D.; Moselund, K. E.; Schmid, H.; Borg, M.; Olziersky, A.; Riel, H. Complementary III−V Heterojunction Lateral NW Tunnel FET Technology on Si. In *2016 IEEE Symposium on VLSI Technology*; IEEE, 2016; Vol. *xx*, pp 1−2.
(30) Schmid, H.; Cutaia, D.; Gooth, J.; Wirths, S.; Bologna, N.; Moselund, K. E.; Riel, H. Monolithic Integration of Multiple III-V Semiconductors on Si for MOSFETs and TFETs. In *2016 IEEE International Electron Devices Meeting (IEDM)*; IEEE, 2016; pp 3.6.1−3.6.4.
(31) Knoedler, M.; Bologna, N.; Schmid, H.; Borg, M.; Moselund, K. E.; Wirths, S.; Rossell, M. D.; Riel, H. Observation of Twin-Free GaAs Nanowire Growth Using Template-Assisted Selective Epitaxy. *Cryst. Growth Des.* **2017**, *17*, 6297−6302.
(32) Chen, R.; Tran, T.-T. D.; Ng, K. W.; Ko, W. S.; Chuang, L. C.; Sedgwick, F. G.; Chang-Hasnain, C. Nanolasers Grown on Silicon. *Nat. Photonics* **2011**, *5*, 170−175.
(33) Shi, B.; Zhu, S.; Li, Q.; Tang, C. W.; Wan, Y.; Hu, E. L.; Lau, K. M. 1.55 μm Room-Temperature Lasing from Subwavelength Quantum-Dot Microdisks Directly Grown on (001) Si. *Appl. Phys. Lett.* **2017**, *110*, 121109.
(34) Wan, Y.; Li, Q.; Liu, A. Y.; Gossard, A. C.; Bowers, J. E.; Hu, E. L.; Lau, K. M. Temperature Characteristics of Epitaxially Grown InAs Quantum Dot Micro-Disk Lasers on Silicon for on-Chip Light Sources. *Appl. Phys. Lett.* **2016**, *109*, 11104.
(35) Ide, T.; Baba, T.; Tatebayashi, J.; Iwamoto, S.; Nakaoka, T.; Arakawa, Y. Room Temperature Continuous Wave Lasing in InAs Quantum-Dot Microdisks with Air Cladding. *Opt. Express* **2005**, *13*, 1615−1620.

DOI: 10.1021/acsnano.7b07911
ACS Nano 2018, 12, 2169−2175